Analysis and attribution of total column ozone changes over the Tibetan Plateau during 1979-2017

Yajuan Li[1,2], Martyn P. Chipperfield[2,3], Wuhu Feng[2,4], Sandip S. Dhomse[2,3], Richard J. Pope[2,3], Faquan Li[5], Dong Guo[6]

1 School of Electronic Engineering, Nanjing Xiaozhuang University, Nanjing, China
2 School of Earth and Environment, University of Leeds, Leeds, UK
3 National Centre for Earth Observation, University of Leeds, Leeds, UK
4 National Centre for Atmospheric Science, University of Leeds, UK
5 Wuhan Institute of Physics and Mathematics, Chinese Academy of Sciences, Wuhan, China
6 Key Laboratory of Meteorological Disaster, Ministry of Education/Joint International Research Laboratory of Climate and Environment Change/Collaborative Innovation Center on Forecast and Evaluation of Meteorological Disasters, Nanjing University of Information Science & Technology, Nanjing, China

Abstract: Various observation-based datasets have confirmed positive zonal mean column ozone trends at mid-latitudes as a result of the successful implementation of the Montreal Protocol. However, there is still uncertainty about the longitudinal variation of these trends and the direction and magnitude of ozone changes at low latitudes. Here, we use the extended Copernicus Climate Change Service (C3S) dataset (1979-2017) to investigate the long-term variations in total column ozone (TCO) over the Tibetan Plateau (TP) for different seasons. We use piecewise linear trend (PWLT) and equivalent effective stratospheric chlorine loading (EESC)-based multi-variate regression models with various proxies to attribute the influence of dynamical and chemical processes on the TCO variability. We also compare the seasonal behaviour of the relative total ozone low (TOL) over the TP with the zonal mean at the same latitude.

Both regression models show that the TP column ozone trends change from negative trends from 1979-1996 to small positive trends from 1997-2017, although the later positive trend based on PWLT is not statistically significant. The wintertime positive trend since 1997 is larger than that in summer, but both seasonal TP recovery rates are smaller than the zonal means over the same latitude band. For TP column ozone, both regression models suggest that the geopotential height at 150 hPa (GH150) is a more suitable and realistic dynamical proxy compared to a surface temperature proxy used in some previous studies. Our analysis also shows that the wintertime GH150 plays an important role in determining summertime TCO over the TP through persistence of the ozone signal. For the zonal mean column ozone at this latitude the QBO is nonetheless the dominant dynamical proxy.

We also use a 3-D chemical transport model to diagnose the contributions of different proxies for the TP region. The role of GH150 variability is illustrated by using two sensitivity experiments

with repeating dynamics of 2004 and 2008. The simulated ozone profiles clearly show that wintertime TP ozone concentrations are largely controlled by tropics to mid-latitude pathways, whereas in summer variations associated with tropical processes play an important role. These model results confirm that the long-term trends of TCO over the TP are dominated by different processes in winter and summer. The different TP recovery rates relative to the zonal means at the same latitude band are largely determined by wintertime dynamical processes.

1 Introduction

The Tibetan Plateau (TP), also known as the third pole, is one of the areas most sensitive to global climate change. It exerts important thermal and dynamical effects on the general circulation and climate change (Yanai et al., 1992; Ye and Wu, 1998). Furthermore, climate changes over the TP have a significant impact on the distribution of stratospheric ozone. By acting as an important greenhouse gas and ultraviolet radiation absorber, variation of the ozone amount and distribution will modify the radiative structure of the atmosphere over the plateau, thereby influencing the climate, ecosystem and human activities (Forster and Shine, 1997; Hartmann et al., 2000).

Using observations from the Total Ozone Mapping Spectrometer (TOMS) satellite instrument, a persistent summertime total column ozone low (TOL) centred over the TP was reported by Zhou et al. (1995). Later studies using satellite and ozonesonde data also found the ozone low in other seasons but with different magnitudes (Zheng et al., 2004; Bian et al., 2006; Tobo et al., 2008). Zou (1996) analyzed total ozone seasonal variations and trends over the TP and showed that relative to zonal mean values, the largest ozone deficit occurs in May, while the smallest deficit occurs in wintertime. They also reported a negative correlation between the ozone deficits and the heat flux from the surface to the air over the plateau. Ye and Xu (2003) also confirmed the persistent existence of the TOL over the TP. They proposed that the high topography and the elevated heating source associated with thermally forced circulations are the two main reasons for its occurrence. In addition, previous observational and modelling studies have suggested that the thermal-dynamical forcing of the TP, for example by air expansion, uplifting of the tropopause, thermal convection, and monsoon circulation, makes a dominant contribution to the TOL especially in summer (e.g. Tian et al., 2008; Bian et al., 2011; Guo et al., 2012, 2015). However, the exact coupling pathways between the thermal-dynamical forcing and long-term total column ozone (TCO) changes during different seasons are still not well established.

It is well known that Antarctic stratospheric ozone decreased severely due to anthropogenic emissions of ozone-depleting substances (ODS) from the 1980s onwards (e.g. Farman et al., 1985). Also, following the implementation of the Montreal Protocol in 1987, signs of an ozone recovery have been reported in recent years (e.g. Chipperfield et al., 2015, 2017; Solomon et al., 2016; Weber et al., 2018). Outside of the polar region, column ozone amounts are largely determined by the stratospheric dynamics and hence quantifying long-term trends is quite challenging (e.g. Rex et al., 2004; Harris et al., 2008; Zhang et al., 2018, 2019). Observations and model simulations indicate that the variability and long-term ozone trends are significantly different at different latitudes (e.g. Austin et al., 2010; Chipperfield et al., 2017, 2018). Major factors contributing to short- and long-term ozone variations include changes in ODS emissions,

atmospheric dynamics, solar irradiance and volcanic aerosols (e.g. WMO, 2014 and references therein).

Previous studies have also documented that TP trends can be affected significantly by internal variabilities. Zou (1996) reported strong negative ozone trends over Tibet for the 1979-1991 time period. The effects of the quasi-biennial oscillation (QBO) and the El Niño-Southern Oscillation (ENSO) on TCO over Tibet were analyzed in subsequent studies (e.g. Zou et al., 2000, 2001). The stratospheric ozone abundance can also be influenced by long-term variations in volcanic aerosols and solar radiation (e.g. Soukharev and Hood, 2006; Fioletov, 2009; Dhomse et al., 2011, 2015, 2016). Besides these traditional explanatory factors, some dynamical proxies, e.g., temperature and geopotential height (GH) have been shown to have significant influence on the long-term ozone variations and effectively help better estimation of ozone trends (e.g. Ziemke et al., 1997; Dhomse et al., 2006). Zhou and Zhang (2005) presented decadal ozone trends over the TP using the merged TOMS/SBUV ozone data over the period 1979-2002 and found that the downward trends are closely related to the long-term changes of temperature and geopotential height. Zhou et al. (2013) found substantial downward ozone trends in the merged TOMS/SBUV ozone data (1979-2010) during the winter-spring seasons over the TP. They also showed that long-term ozone variations are largely correlated with thermal-dynamical proxies such as the lower stratospheric temperatures, with its contribution reaching around 10% of the total ozone change. Zhang et al. (2014) indicated that the TOL over the TP in winter has deepened during the period 1979-2009 and the thermal-dynamical processes associated with the TP warming (increasing surface temperature) may account for more than 50% of the TCO decline in this region.

Many previous studies have demonstrated the contributions of dynamical processes to the long-term ozone variation in different latitude bands (e.g. Dhomse et al., 2006; Chehade et al., 2014) as well as the TP region (e.g. Zhou et al., 2013; Zhang et al., 2014). As we know that wintertime stratospheric circulation has large interannual variability that is mainly driven by tropospheric processes, the choice of dynamical proxy for this tropospheric influence varies for different latitude bands. For mid-high latitudes, most studies use the Eliassen-Palm Flux (or heat flux) to explain a large part of dynamical variability (e.g. Weber et al, 2003). However, heat flux is not a suitable dynamical proxy for subtropical latitudes (e.g. Fusco and Salby, 1999; Hood and Soukharev, 2005; Dhomse et al., 2006) as transport in this region is balanced by tropical upwelling and isentropic transport in the lower stratosphere. Hence a better proxy is needed to explain the dynamical influence for the TP region.

Under the background of global surface warming, concern about regional climate changes have been focused on high-elevation areas, such as the Tibetan Plateau. The geopotential height in the free atmosphere is an important thermal-dynamical proxy that not only conveys information about the thermal structure of the atmosphere, but also serves as an indicator of synoptic circulation changes (Christidis and Stott, 2015). The natural and anthropogenic contributions to the changes in GH establish the coherent thermal-dynamical nature of externally forced changes in the regional climate system, which provides the basis for the validation of climate models. In this study, the GH at 150 hPa over the TP is used as a new thermal-dynamical proxy which incorporates coupling between the local TP circulation and various tropospheric teleconnection patterns and represents the tropospheric dynamical influence more realistically.

In different seasons, especially in winter and summer, the proxies affecting the ozone variations over the TP may also be different due to some complicated mechanisms. Fioletov and Shepherd (2003) have studied the seasonal persistence of mid-latitude total ozone anomalies and demonstrated that ozone values are correlated through the annual cycle from the buildup in winter-spring to the ozone minimum in autumn. For mid-latitudes, the tropical zonal winds as manifested in the QBO dominate the wintertime ozone buildup (Holton and Tan, 1980). However, such information remains unknown for the large local TP region.

With the extended Copernicus climate change service (C3S) TCO time series available from 1979 to early 2018, the aim of this paper is to study the long-term ozone trend and variability over the Tibetan region. Based on statistical regression analysis of C3S ozone data and TOMCAT/SLIMCAT three-dimensional (3-D) chemical transport model (CTM) simulations, the contributions of different influencing variables including the local thermal-dynamical proxy (GH) are diagnose to help understand the long-term ozone variability in different seasons and over different areas.

The layout of the paper is as follows. Section 2 introduces the C3S ozone dataset and TOMCAT/SLIMCAT model used for the analysis of the total ozone variability. The long-term TCO time series and TOL over the TP region are presented in Section 3. Regression models as well as analysis of the contribution of different proxies to the total ozone variations in different seasons are given in Section 4. Section 5 discusses sensitivity experiment results based on TOMCAT/SLIMCAT and is followed by our summary and conclusions in Section 6.

2 Data

2.1 Ozone dataset from C3S

High quality observational based datasets are necessary for better quantification of decadal TCO trends. This is because interannual variability can cause variations of up to 20% whereas ozone trends are generally less than half a percent. As the lifetime of most satellite instruments is less than two decades, merged satellite datasets are widely used to determine long-term ozone trends. These datasets are created by combining total ozone measurements from different individual instruments to provide global coverage over several decades (e.g. Frith et al., 2014). The Solar Backscatter Ultraviolet (SBUV) provides nearly continuous satellite-based measurements of total ozone to analyze trends. The variations from all the instruments are within 2% relative to the ground-based data at all latitudes (Labow et al., 2013). SBUV-merged data is obtained from https://acd-ext.gsfc.nasa.gov/Data_services/merged/instruments.html. However, this merged satellite dataset is available as zonal mean values at 5^{o} latitude resolution, and therefore is not well suited to study relatively small geographical areas such as the TP.

Hence, here we use the total column ozone from the C3S which is produced by the European Centre for Medium-Range Weather Forecasts (ECMWF). For a detailed description and data availability, see https://cds.climate.copernicus.eu/cds. In brief, these are monthly mean gridded data that span from 1970 to present. They are created by combining total ozone data from 15 satellite sensors including GOME (1995-2011), SCIAMACHY (2002-2012), OMI

(2004-present), GOME-2A/B (2007-present), BUV-Nimbus4 (1970-1980), TOMS-EP (1996-2006), SBUV-9, -11, -14, -16, -17, -18, -19 (1985-present) and OMPS (2012-present). The horizontal resolution of the assimilated product after January 1979 is 0.5 ° × 0.5 °. The document describing the methodology adopted for the quality assurance in the C3S-Ozone procurement service, with detailed information about the ground-based measurements used to verify satellite observations, the specific technical project implemented to compare the gridded (level-3) and assimilated (level-4) data, and the metrics developed to associate validation results with user requirements, can be downloaded from https://cds.climate.copernicus.eu/cdsapp#!/dataset/ozone-monthly-gridded-data-from-1970-to-present?tab=doc. The strength of this dataset is the long-term stability of the total column monthly gridded average product that is below the 1%/decade level. Systematic and random errors in this data are below 2% and 3-4%, respectively, hence making it suited for long-term trend analysis. The evaluation of ozone trends performed using merged deseasonalized anomalies is presented in Sofieva et al. (2017) and Steinbrecht et al. (2017). They show that ozone trends are in agreement with those obtained using other datasets, and they are close to those reported in WMO (2014).

We use four different area-weighted total ozone time series during 1979-2017: TP (27.5 °-37.5 °N, 75.5 °-105.5 °E), zonal TP (full zonal mean for 27.5 °-37.5 °N) as well as zonal mean for latitude bands to the south (10 °-20 °N) and north (40 °-50 °N) of the TP region. These regions represent the tropics and mid-latitudes with the TP and zonal TP in the critical zone. We choose them to compare the contribution of different dynamical proxies to their ozone variations especially over the TP region. In this paper, we also use the direct ozone observations from the SBUV series of satellites to validate the results based on C3S.

2.2 TOMCAT/SLIMCAT model

Chemistry-transport models are important tools to investigate how past and present-day ODS and greenhouse gas (GHG) concentrations have influenced the ozone layer (e.g. Shepherd et al., 2014; Zvyagintsev et al., 2015). In combination with observed ozone time series, simulations allow the attribution of ozone changes, thus encapsulating our understanding of the fundamental physics and chemistry that controls ozone and its variations (e.g. Chipperfield et al., 2017). TOMCAT/SLIMCAT (hereafter SLIMCAT) is a 3-D off-line chemical transport model (Chipperfield et al., 2006), which uses winds and temperatures from meteorological analyses (usually ECMWF) to specify the atmospheric transport and temperatures and calculates the abundances of chemical species in the troposphere and stratosphere. The model has the option of detailed chemical schemes for various scenarios with different assumptions of factors affecting ozone (e.g. Feng et al., 2011; Grooss et al., 2018), including the concentrations of major ozone-depleting substances, aerosol effects from volcanic eruptions (e.g. Dhomse et al., 2015), and variations in solar forcing (e.g., Dhomse et al., 2013; 2016) and surface conditions. For this study, the model has been forced by ECMWF ERA-Interim reanalysis (Dee et al., 2010) and run from 1979-2017 at a horizontal resolution of 2.8 ° × 2.8 °with 32 levels (up to around 60 km).

We perform control and sensitivity simulations based on the SLIMCAT CTM to elucidate the impact of dynamical changes on the total ozone variations over the TP region. The control experiment R1 uses standard chemical and dynamical parameters for the time period 1979-2017, which is identical to the control run of Chipperfield et al. (2017). To understand the special

dynamical influences (e.g. GH) on ozone variations over the TP, two sensitivity experiments R2 and R3 were performed with all configurations the same as R1 except the simulations used annually repeating meteorology for the years 2004 and 2008, respectively. These years were chosen because the 150 hPa GH in wintertime is substantially different while other dynamical proxies are almost the same for the two years. We also take a 5-year average from model dates 2004-2008 for each sensitivity experiment to exclude the influence from other time-dependent changes (e.g. chemical processes).

3 TCO and TOL over the TP

Figure 1 shows the TCO time series averaged for December-January-February (DJF) and June-July-August (JJA) seasons during 1979-2017 over the North-TP (40 °-50 °N), South-TP (10 °-20 °N), zonal-TP region (27.5 °-37.5 °N) and the TP region (27.5 °-37.5 °N, 75.5 °-105.5 °E). Zonal mean values from SBUV-merged total ozone data for same latitude band are also shown in **Figures 1** (a) and (b) to compare with the C3S datasets. Differences between C3S and SBUV are less than 2-3% throughout the data record and are shown in **Figure S1,** confirming that there is no long-term drift in the C3S data**.** As shown in **Figure 1**, the magnitudes of inter-annual variations increase with latitude, with amplitude of DJF ozone variations being much larger than JJA. Besides, **Figures 1** (c) and (d) show the TP and zonal-TP ozone time series, highlighting much smaller difference in DJF (<5 DU) compared to about 20 DU difference in JJA. This is consistent with previous studies (e.g. Ye and Xu, 2003; Zhang et al., 2014).

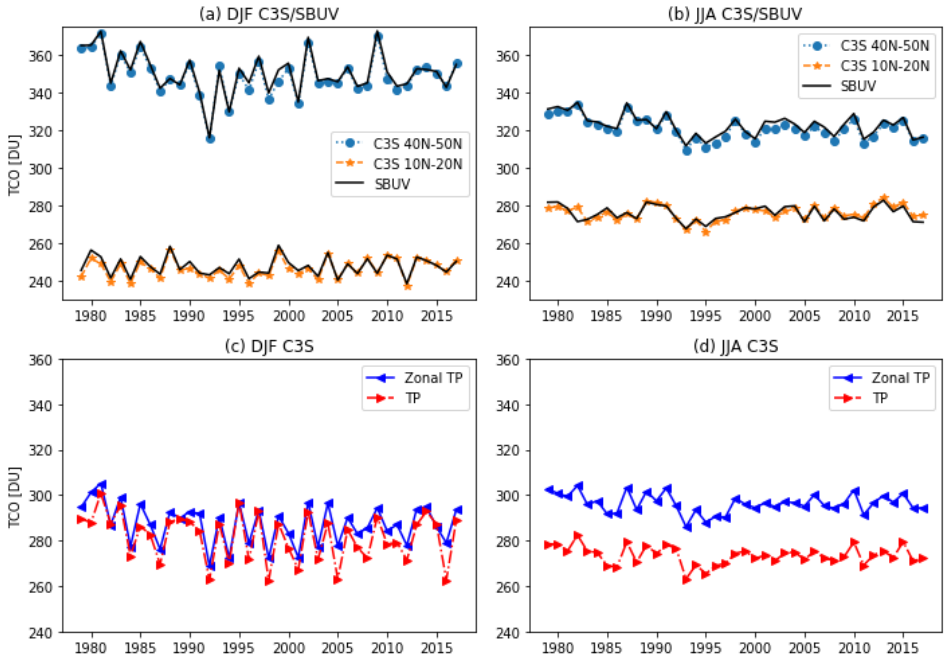

Figure 1. C3S-based total column ozone (TCO) time series averaged for December-January-February (DJF) and June-July-August (JJA) seasons during 1979-2017 over (a, b) the North-TP (40 °-50 °N), and South-TP (10 °-20 °N) regions, and (c, d) the zonal-TP (27.5 °-37.5 °N) and the TP regions (27.5 °-37.5 °N,

75.5 °-105.5 °E). Panels (a) and (b) also show the satellite-based observations from SBUV (black solid lines).

To illustrate TOL characteristics, we calculate the zonal deviations by subtracting the zonal mean total ozone for each latitude band from the TCO at each grid point (**Figure 2)**. The negative zonal deviations suggest that the TOL centred over the TP exists for all the seasons. As shown in **Figures 1 (c) and (d)**, TOL over the TP is most discernible in summer (JJA), followed by spring (March-April-May, MAM) and autumn (September-October-November, SON), while weakest in winter (DJF). The TOL centre also moves from the northwest in spring (MAM) to the south in winter (DJF). The mechanisms for these seasonal differences over the TP are very different in winter and summer. In wintertime, the plateau geographic effect is somewhat less effective in modifying the lower stratospheric circulation as the subtropical jet moves southwards (e.g. Luo et al., 2019). During summertime, the TP is an elevated heating source causing thermally forced anticyclonic circulation. The upper-level Asian summer monsoon anticyclone coupling with deep convection over the TP can potentially transport ozone-poor air from the boundary layer upward into the upper troposphere and lower stratosphere (Liu et al., 2003; Gettelman et al., 2004; Randel and Park, 2006; Bian et al., 2011). Seasonal variations in TCO over the TP and zonal-TP region are shown in **Figure S2**. The wintertime ozone buildup and steady summertime ozone decline are evident over both regions. However, the high topography of the TP causes an earlier phase (about 1 month) and smaller amplitudes in TCO variability over the TP. The different TOL magnitudes in different seasons could be associated with the fact that wintertime ozone concentrations are largely controlled by large-scale dynamical processes, while photochemical loss is the only dominant process in summer. Thus, it is necessary to analyze the influences of the chemical and dynamical processes (e.g. EESC, solar, QBO and the local thermal-dynamical proxy) on the total ozone variability under different atmospheric conditions.

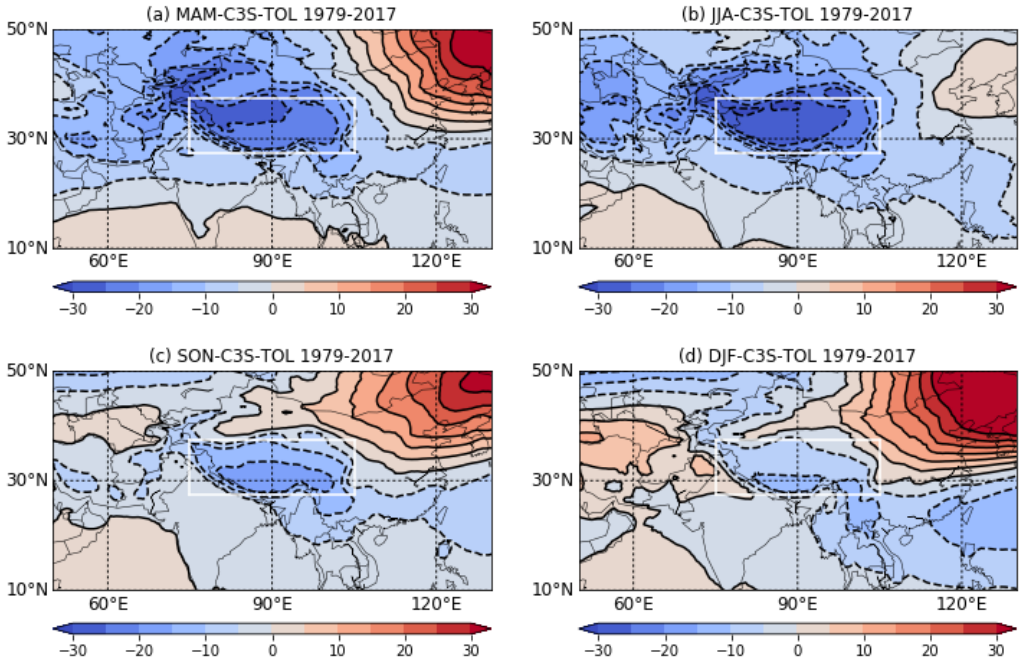

Figure 2. Latitude-longitude cross section of the zonal ozone deviations for (a) March-April-May (MAM),

(b) June-July-August (JJA), (c) September-October-November (SON) and (d) December-January-February (DJF) seasons based on C3S total ozone dataset for 1979-2017 time period. The solid and dashed contours represent the positive and negative zonal deviations. The contour interval is 5 DU. The TP region (27.5 °-37.5 °N, 75.5 °-105.5 °E) is marked by the white rectangle.

4 Multi-variate linear regression based on C3S

4.1 Regression models

Multi-variate linear regression models are widely used to assess the long-term total ozone trends. In these models, proxies are included to separate the influences of important short- and long-term processes on trend determination. Typically, multi-variate linear regression models use Equivalent Effective Stratospheric Chlorine (EESC) or piecewise linear trend (PWLT) terms for long term ozone trends (e.g. Reinsel et al., 2002; Nair et al., 2013; Chehade et al., 2014). EESC is a measure of the total inorganic chlorine and bromine amounts in the stratosphere, which drive chemical ozone depletion. Previous studies have indicated that EESC is a main contributor to the long-term global ozone decline and the trend changes after the end of 1990s (e.g. Newman et al., 2004; Fioletov and Shepherd, 2005; Randel and Wu, 2007). We use this method to study the effect of EESC on the long-term ozone variations over the TP and the other zonal regions. A PWLT-based regression method is used to statistically analyze robustness of decreasing and recovery trends in the total ozone before and after the EESC peak in 1997. Our aim is to clarify statistical significance of the key processes responsible for the total column ozone variations over the TP in different seasons, using two different regression models.

Traditional explanatory proxies to account for influence of chemical and dynamical processes, include the F10.7 solar flux for the 11-year solar cycle, quasi-biennial oscillation (QBO) at 30 hPa and 10 hPa (QBO30 and QBO10), and El-Nino Southern Oscillation (ENSO) (e.g. Baldwin et al. 2001; Camp and Tung, 2007). Some studies also include aerosol optical depth at 550 nm, to account for ozone loss due to volcanically enhanced stratospheric aerosol loading after El-Chichón (1982) and Mt. Pinatubo (1991) eruptions. To account for dynamical variability typical indices are wind near vortex, Arctic oscillation (AO) index, Ellison Palm Flux or eddy heat flux (e.g. Chehade et al., 2014 and references therein). Due to unique nature of TP orography, the local thermal-dynamical forcing, e.g. the geopotential height at 150 hPa (GH150) and the surface temperature (ST) are also considered as dynamical proxies. We calculate the GH150 and ST over the TP and zonal latitude bands from the ECMWF ERA-Interim reanalysis dataset obtained via https://apps.ecmwf.int/datasets/data/interim-full-daily/ (last access: 10 January 2020). Radiosonde-based GH150 data from a nearby Lhasa station (http://weather.uwyo.edu/upperair/seasia.html) are also used for comparison with ECMWF data (**Figure S3**). The statistically significant correlation (0.96) validates our use of the ECMWF GH150 data for TP region.

Table 1. Correlation coefficients for the DJF mean TCO and explanatory variables over the TP during 1979-2017

	EESC	**Solar**	**QBO30**	**QBO10**	**ENSO**	**Aerosol**	**AO**	**ST**	**GH150**
TCO	**-0.324 ****	**0.247**	**-0.411 *****	**-0.560 *****	**0.256**	**0.048**	**-0.124**	**-0.256**	**-0.514 *****
EESC	1.0	-0.196	0.029	0.040	-0.064	-0.138	0.120	-0.057	-0.058
Solar		1.0	0.011	0.060	0.035	0.234	0.398 ***	-0.089	0.069
QBO30			1.0	0.011	0.006	-0.035	0.222	-0.072	0.163
QBO10				1.0	-0.011	0.219	0.100	-0.069	0.096
ENSO					1.0	0.372 **	-0.180	-0.089	-0.468 ***
Aerosol						1.0	0.216	-0.309 **	-0.214
AO							1.0	-0.104	0.374 **
ST								1.0	0.618 ***
GH150									1.0

*** 99% confidence level; ** 95% confidence level

Due to the large differences in scales and units of the explanatory variables, we have standardized all the time series to ensure each factor contributes approximately proportionately to the final ozone variations. The transformation does not change the correlation and fitting coefficients. Another important criterion for multi-variate regression model is that explanatory variables should not be highly correlated with each other. **Table 1** shows the correlation values for the DJF mean TCO (over the TP region) and explanatory variables during 1979-2017 (a similar analysis for JJA is presented in the supplementary **Table S1**). The local thermal-dynamical proxy (GH150 or ST over the TP) is de-trended before being used in the regression models. As shown from the correlation analysis, the DJF mean TCO has significant negative correlations with EESC, QBO and GH150. The solar variability proxy (F10.7 index) is strongly correlated with the AO (0.398) time series. Also, the GH150 time series shows relatively stronger correlation with the ENSO (-0.468), AO (0.374), and ST (0.618) time series. We also find that aerosol and ENSO are correlated (0.372). Hence, to avoid any aliasing effects, we omit the data after El-Chichón (1982, 1983) and Mt. Pinatubo (1991, 1992) volcanic eruptions. AO is also removed as it shows strong correlation with the solar and GH150 proxies. As for the other partially correlated proxies (ENSO, ST and GH150), we make three groups of independent variables to analyze the TCO variations and compare the corresponding regression results under different situations:

$$TCO(t) = C_0 + C_1 \cdot EESC(t) + C_2 \cdot solar(t) + C_3 \cdot QBO(t) + C_4 \cdot ENSO(t) + \varepsilon(t) \quad (1)$$

$$TCO(t) = C_0 + C_1 \cdot EESC(t) + C_2 \cdot solar(t) + C_3 \cdot QBO(t) + C_4 \cdot ENSO(t) + C_5 \cdot ST(t) + \varepsilon(t) \quad (2)$$

$$TCO(t) = C_0 + C_1 \cdot EESC(t) + C_2 \cdot solar(t) + C_3 \cdot QBO(t) + C_4 \cdot GH150(t) + \varepsilon(t) \quad (3)$$

where *t* is a running index corresponding to the years during the period 1979-2017, excluding the four years due to the volcanic aerosol loading. *QBO* herein is equivalent to ($a \times QBO30 + b \times QBO10$). C_0 is a constant for the long-term average. C_1-C_5 represent the time-dependent regression coefficients of each proxy and ε is the residual. In the PWLT regression model, the $C_1 \times EESC(t)$ term is replaced by ($c1 \times t1 + c2 \times t2$) in Eq. (1-3) with linear trends *(Trend1 and Trend2)* in the periods 1979–1996 and 1997–2017, respectively.

4.2 Regression analysis

We apply the multi-variate linear regression models to the seasonal mean TCO time series to determine long-term ozone changes over the TP, zonal-TP, South-TP and North-TP zonal bands, respectively. **Table 2** lists the adjusted determination coefficients (Adj. R-squared) based on PWLT regression model for DJF mean TCO time series with three groups of independent explanatory variables over four different regions. Compared to the regression results based on Eq. (1), the additional consideration of the ST proxy in Eq. (2) improves the adjusted R-squared over all these regions, especially over the TP. By replacing ENSO in Eq. (1), the GH150 in Eq. (3) improves the regression fit more significantly for the TP and zonal-TP time series compared to the ST. However, similar improvements are not visible for the non-TP zonal time series. This seems more feasible as the changes in GH150 represent locally relevant dynamical variability that is modulated by the orography and local circulations over the TP. EESC-based regression results with adjusted determination coefficients are also shown in the supplementary **Table S2**, and are consistent with PWLT-based regression results in **Table 2**.

Table 2. Adjusted determination coefficients of PWLT-based regression model for DJF mean TCO over different regions with different proxies

DJF TCO (Adj. R-squared)	PWLT, solar, QBO, **ENSO** based on Eq. (1)	PWLT, solar, QBO, **ENSO, ST** based on Eq. (2)	PWLT, solar, QBO, **GH150** based on Eq. (3)
TP, 27.5 ℃N -37.5 ℃N, 75.5 ℃E -105.5 ℃E	**0.56**	**0.68**	**0.75**
North-TP, 40 ℃N -50 ℃N	0.55	0.56	0.54
Zonal-TP, 27.5 ℃N -37.5 ℃N	**0.64**	**0.69**	**0.74**
South-TP, 10 ℃N -20 ℃N	0.64	0.70	0.67

Using the PWLT-based regression model, we analyze the TCO trends for 1979-1996 and 1997-2017. The fitted signals of the TCO anomalies and explanatory terms in Eq. (3) for DJF and JJA are shown in **Figure 3**, and corresponding regression coefficients along with 2σ standard deviations are listed in **Table 3.** As the summer/autumn time ozone variability is much weaker compared to seasonal ozone buildup during winter and spring, the long-term ozone anomalies as

well as the contributions from different explanatory variables show much weaker contribution in JJA. Hence, the adjusted determination coefficient in JJA mean TCO regression (0.61) is also much smaller. As expected, linear trends in both DJF and JJA show a decline over the TP during 1979-1996 (Trend1) and a recovery since 1997 (Trend2). Furthermore, the upward trend since 1997 in JJA is relatively weaker than that in DJF. EESC-related ozone trends over the TP and zonal-TP region in both seasons are given in the supplementary **Table S3**. The TCO trends over the TP, compared to those over the zonal-TP region, show relatively smaller decline and recovery rates before and after 1997. These differences indicate the zonal asymmetry in ozone trends due to longitudinal variations. The comparison between the EESC and PWLT trends shows a good agreement, except that EESC trends are statistically significant within 2σ due to the full data record, however, the positive trends (Trend2 term) in PWLT are always non-significant, highlighting complexities in determination of ozone trends at low latitudes.

Except for the linear trends, all the other explanatory proxies (solar cycle, QBO and GH150) contribute significantly to the ozone variations in DJF (above the 99% confidence level), especially combined contribution from three dynamical proxies (QBO30, QBO10 and GH150) which adds up to 40 DU. As shown later JJA ozone concentration are largely controlled by photochemical ozone loss, contribution from GH150 drops sharply (~ 0.27 DU). Hence, main contributors to the JJA mean TCO variations are linear trends (7.86 DU), solar cycle (4.61 DU) and QBO at 10 hPa (6.56 DU). Results obtained from the EESC-based regression model (not shown) are very similar to those shown in **Table 3**, confirming the robustness of the results.

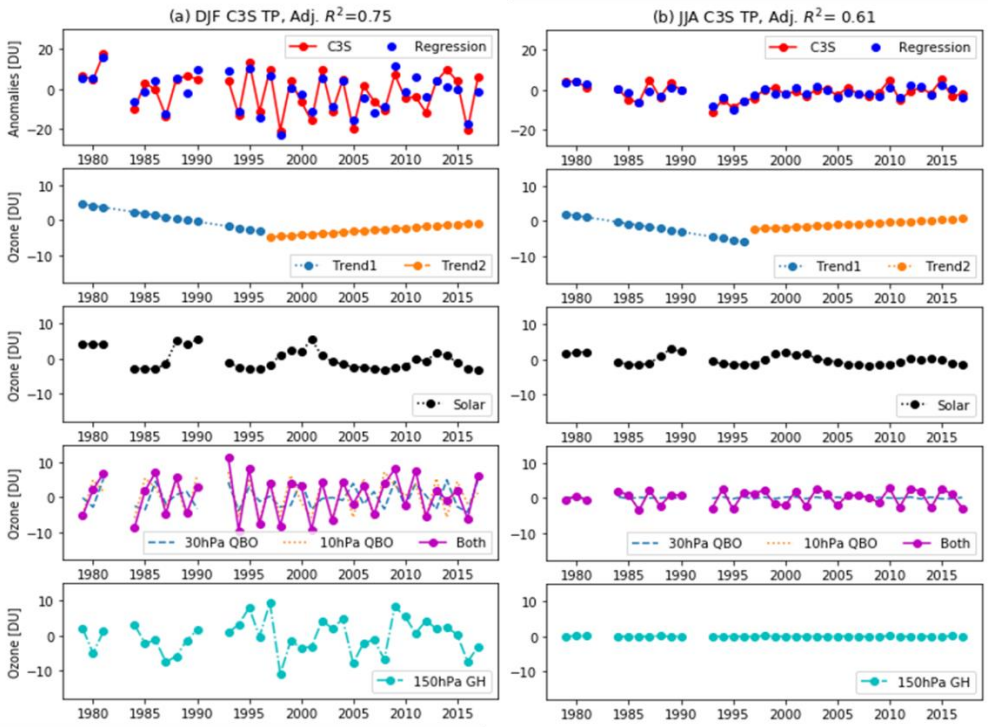

Figure 3. (a) PWLT regression results with contributions from linear trends for 1979-1996 and 1997-2017 time periods, solar cycle, QBO at 30 hPa and 10 hPa, and the GH at 150 hPa in DJF based on C3S during 1979-2017 over the TP region; (b) Similar to (a) but with all factors averaged in JJA.

Table 3. PWLT-based regression coefficients and standard deviations for the DJF and JJA mean TCO over the TP during 1979-2017

PWLT Regression	DJF, Adj. R^2=0.75 coef ± std err (2σ)	|p|>t	JJA, Adj. R^2=0.61 coef ± std err (2σ)	|p|>t
Trend1	-0.45±0.28	0.118	-0.46±0.13	0.002
Trend2	0.20±0.19	0.311	0.15±0.09	0.126
Solar	2.87±0.99	0.008	1.40±0.49	0.008
QBO30	-3.27±0.94	0.002	-0.20±0.40	0.614
QBO10	-5.05±0.89	0.000	2.11±0.44	0.000
GH150	-4.67±0.90	0.000	0.06±0.46	0.893

To describe quantitatively the contributions of different explanatory proxies to the DJF and JJA mean total ozone variability over different regions, we calculate the percentage ozone change for comparison, as shown in **Figure 4**. These contributions using percentage ozone change are represented by Eq. (4):

$$\Delta TCO[\%] = \frac{\max(X[DU]) - \min(X[DU])}{mean(TCO[DU])} \times 100\% \quad (4)$$

where X means the contribution of one proxy (in DU) to the long-term ozone variability. In **Figure 4**, the percentage contribution with an error bar indicates the statistical significance within 2σ. During the wintertime (DJF), dynamical proxies (QBO and GH150) exert a significant effect on the total ozone variability over the TP (about 8% each), while QBO dominates over the zonal-TP region (up to 7%). However, in summertime (JJA), contributions from dynamical proxies are much smaller; although the contribution from the QBO10 remains above 2%, the contribution from GH150 almost disappears.

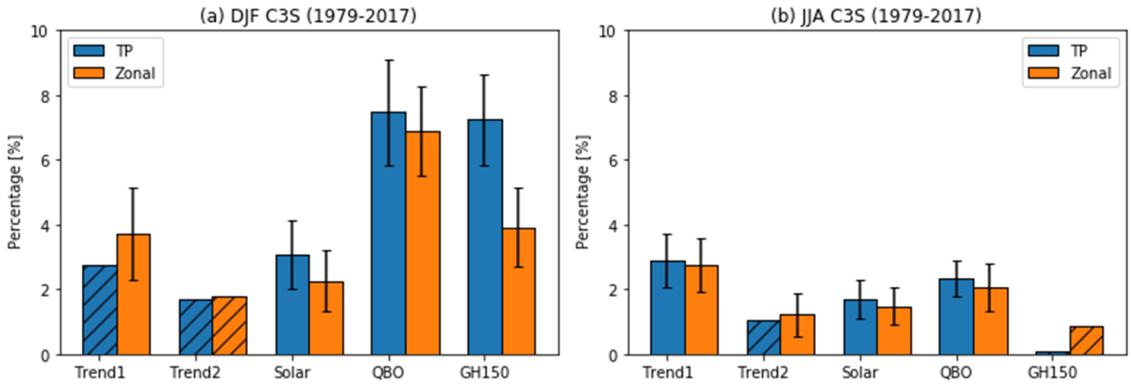

Figure 4. Peak contributions of various explanatory variables to variability in the total ozone column (in %) in (a) DJF and (b) JJA over the TP and the zonal-TP region based on C3S data during 1979-2017. The hatched bars without error bars indicate the contribution is not significant within 2σ level.

Previous studies have found that changes in GH150 associated with an enhanced South Asian high (SAH) results in significant TCO deviations at 150-50 hPa over the TP (Tian et al., 2008; Bian et al., 2011; Guo et al. 2012). From April onwards, as the SAH advances over the TP, summertime GH150 starts increasing (**Figure S4**). Between the TP and zonal-TP region the GH150 contribution shows a maximum difference in May when the negative TOL is also strongest (**Figure S2**), with a correlation coefficient of -0.86 within the 0.001 significance level. Thus, the amplitude of SAH imposes an important constraint on the formation of the summertime TOL over the TP. However, here we find that GH150 makes a major contribution to the TCO variability in wintertime but not in summertime. The sharp contrast between the contributions of the 150 hPa GH in DJF and JJA is an interesting feature and a possible explanation for those differences is discussed below.

The seasonal variability in TCO over the TP (**Figure S2**) indicates a marked seasonal cycle with a buildup of total ozone through the winter and a decline through the summer. The correlation of the DJF mean TCO with the subsequent JJA means over the TP during 1979-2017 is 0.44, which is statistically significant above the 95% confidence level. This significant positive correlation indicates that negative or positive wintertime TCO anomalies over the TP appear to persist through the summer period (as shown in **Figure 5**). **Table 4** lists the correlation coefficients of TCO variations in a given season of the year with those in subsequent seasons. The correlation decreases from the buildup in winter to the end of summer and there exists a sharp drop between the summer (JJA) and autumn (SON) which may reflect that dynamical variability is nearly absent during summer months and ozone simply drops off photochemically in a predictable way (Fioletov and Shepherd, 2003). Detailed analysis of the correlation between subsequent months of the year is provided in the supplementary information **Table S4**.

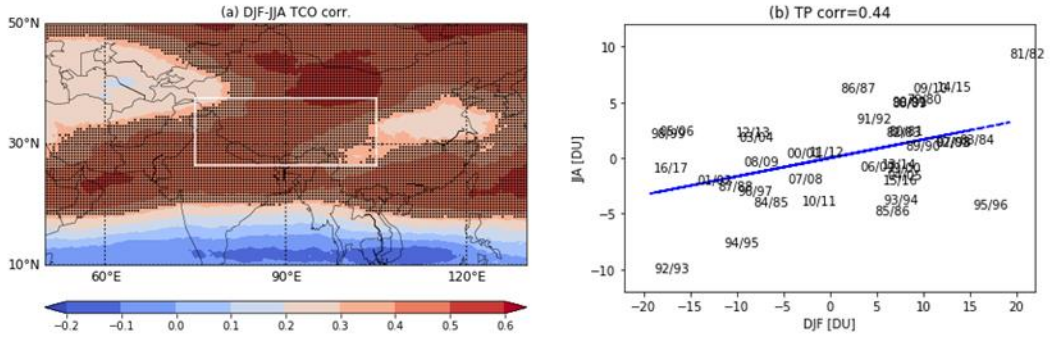

Figure 5. (a) Correlation map of the DJF and JJA mean TCO based on C3S during 1979-2017. Correlation values in the stippled area are statistically significant above the 95% confidence level. The white rectangle represents the TP region. (b) Correlation fit between the DJF and JJA mean ozone anomalies (DU) during 1979-2017 over the TP region.

Table 4. Correlation coefficient between ozone values in a given season and the subsequent season

lags	1	2	3
SON	**0.626**	**0.537**	**0.345**
DJF	**0.812**	**0.440**	-0.217
MAM	**0.662**	0.053	-0.158
JJA	**0.413**	0.018	0.058

1 lag=3 months, bolded numbers are statistically significant within 2σ

Fioletov and Shepherd (2003) highlighted the seasonal persistence of mid-latitude total ozone anomalies and indicated that seasonal predictability is applicable for latitudinal belts or large regions only. The seasonal persistence of ozone anomalies over the TP also implies a causal link between the wintertime ozone buildup due to planetary-wave induced transport and the subsequent chemical loss. The ozone buildup in wintertime when transport dominates is largely modulated by QBO (Holtan and Tan, 1980). However, GH150 represents large part of wintertime variability in the ozone transport. In summertime, as expected, photochemical processes become more important while dynamical impact from QBO decreases and almost disappears for GH150. Seasonal persistence in TCO anomalies shows that if there is more transport in DJF as represented by GH150 changes, higher ozone values will persist for at least 6 months, even though there is little correlation between summertime ozone anomalies and GH150. This analysis clearly highlights dynamical influence of the wintertime GH150 on the summertime (JJA) ozone concentrations.

5 Model Sensitivity Simulations

To investigate the role of wintertime GH150 on ozone transport, we use the SLIMCAT 3-D chemical transport model to understand its role under different conditions. The simulated TCO time series obtained from the control experiment R1 are shown in the supplementary **Figure S5**. Overall, modelled TCO are consistent with the C3S-based TCO data although they are low biased. By applying the PWLT regression model in Eq. (3) to the simulated TCO time series, the percentage ozone change from each explanatory proxy is shown in **Figure S6**. The simulation results are similar to the C3S regression results, although contributions from most explanatory proxies are larger except for the GH150. This difference is probably due to the coarse model resolution and the inhomogeneities in ERA-Interim data, especially before 2000 (e.g. Dhomse et al., 2011, 2013; McLandress et al., 2014). The contribution of the GH150 proxy to the simulated TCO variations over the TP is statistically significant in DJF but not in JJA. To further elucidate the role GH150 plays in the total ozone variability over the TP, we performed two sensitivity experiments (R2 and R3) with repeating dynamics from years 2004 and 2008, respectively. For the two years, the wintertime difference in QBO is modest but GH150 is significantly different. We then take a 5-year average based on a time-slice simulation during 2004-2008 for each sensitivity experiment to ensure that other chemical factors (EESC, solar cycle etc.) are the same between the simulations. Thus, the model settles down with the GH150 as the main proxy that influences the ozone variations over the TP.

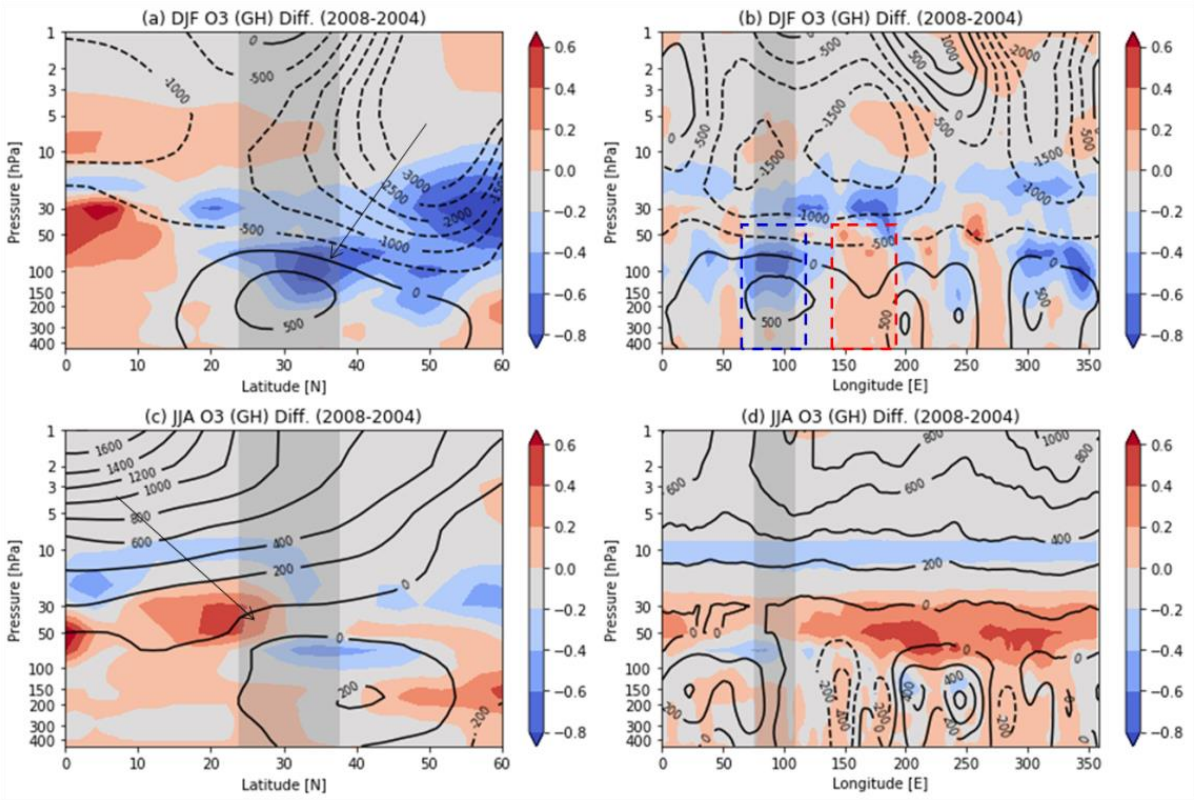

Figure 6. (a) Pressure-latitude and (b) pressure-longitude cross section of DJF mean ozone differences (colours in DU) between the 5-year averaged SLIMCAT sensitivity experiments R2 and R3, and the geopotential height (GH) differences (contours in gpm) between the years 2004 and 2008. (c, d) Similar to (a, b) but averaged for JJA. Positive ozone and GH differences are shown with red colours and solid contours, whereas blue colours and dashed contours indicate negative differences. The shaded area shows the TP region averaged over the 75.5 °-105.5 °E longitude band (a, c) and the 27.5 °-37.5 °N latitude band (b, d). The arrows in (a) and (c) indicate the TP GH differences influenced by those from the high and low latitudes; the dashed blue and red boxes in (b) indicate the negative and positive ozone anomalies over the TP and the Pacific Ocean.

A caveat is that none of the dynamical processes is independent. The GH150 proxy represents the overall tropospheric dynamical influence somewhat realistically as it incorporates coupling between various tropospheric teleconnection patterns and the local TP circulation. To better understand the zonal and meridional pathways, the vertical DJF mean GH differences between the years 2004 and 2008 as well as the 5-year averaged ozone differences (2004-2008) based on the SLIMCAT sensitivity simulations are represented by the contours and colours in **Figure 6**. The shaded area shows the TP region. In DJF (**Figures 6** (a) and (b)), a positive anomaly centre of the GH difference occurs near the 150 hPa pressure level, co-located with a negative ozone anomaly. In JJA (**Figures 6** (c) and (d)) there are no such clear anomaly centres for mean GH and ozone differences over the TP.

By comparing the GH variation with latitude in **Figures 6** (a) and (c), we find that the DJF mean GH differences over the TP are mainly influenced by those over the high latitudes, and in JJA they

are mainly influenced by those from low latitudes (as shown by the arrows therein). This may be because the TP lies near the boundary between the tropics and mid-latitudes in the troposphere. Due to the movement of the Inter Tropical Convergence Zone (ITCZ), the TP in wintertime is located in mid-latitude band where ozone variability is determined by the tropopause height or folds in the lower stratosphere, while in summer, the TP lies in the tropical band where ozone variability is largely determined by QBO (and QBO-induced circulation) in the mid-stratosphere (Baldwin et al., 2001).

The GH variation with longitude in **Figures 6** (b) and (d) suggests a tropospheric coupling between the local TP circulation and some tropospheric teleconnection patterns (e.g. ENSO or Walker circulation). As the TP is an elevated heat source, the differences in heat distribution between the plateau and ocean will cause air motions in the zonal and vertical direction. In the normal condition, the pressure gradient force that results from a high-pressure system over the eastern Pacific Ocean and a low-pressure system over the TP will cause the global general circulation (such as Walker circulation) and therefore affect the ozone distribution. A correlation analysis shows that the GH150 proxy over the TP is in a strong, negative relation to ENSO in DJF, which means during an El Niño event GH150 near the TP also increases, thereby increasing tropopause height, leading to a decrease in TCO over the TP. The positive-negative vertical band-like features in DJF mean ozone differences shown in **Figure 6** (b) seem to closely resemble Walker-circulation-type anomalies (Hu et al., 2016). They also explain why the ozone differences over the TP and the Pacific Ocean are opposite in sign, as indicated by the dashed blue and red boxes therein. Thus, we suggest that wintertime GH fluctuations associated with ENSO events or Walker circulation may play an important role in controlling the TCO variability over the TP. In JJA, however, there are no distinctive features of GH and ozone differences near the TP. As the summertime ozone is less controlled by the dynamical processes (especially GH150), there would not exist such a clear correlation as that in wintertime. Overall, the model results support the hypothesis that wintertime TP ozone variations are largely controlled by tropics-to-high latitude transport processes whereas summertime concentrations result from the combined effect of photochemical decay and tropical processes.

6 Summary and Conclusions

In this study, we have analyzed the variations and trends of the total column ozone and the relative total ozone low over the Tibetan Plateau in different seasons during the period 1979–2017. The most recent C3S datasets based on model assimilation of meteorological and ozone observations are used and compared with merged SBUV satellite observations. We use the PWLT- and EESC-based multi-variate regression models to analyze the contributions and trends associated with the dynamical and chemical processes that modify the total ozone changes over the TP and zonal areas. In addition to conventional regression proxies (EESC, solar cycle, QBO, ENSO etc.), we also use the local thermal-dynamical proxy (ST or GH150) to account for the dynamical influence on the wintertime and summertime ozone changes over the TP. Based on the SLIMCAT 3-D model, we have performed sensitivity experiments to explore the role 150 hPa GH plays in the DJF mean ozone variations over the TP.

Our main conclusions are as follows:

- The comparison of the C3S ozone dataset with the merged SBUV satellite-based observations has verified the feasibility of using assimilated C3S data to study long-term variations over the relatively small TP region.

- With the C3S data extended up to early 2018, the long-term variations of TCO and TOL averaged in different seasons are compared over 1979-2017. The TOL over the TP compared to the zonal mean at the same latitude band exists throughout the year though the magnitude and the centre location change with season. Both PWLT and EESC-based multi-variate regression models show a change in TCO trends from the pre-1997 decline to the post-1997 recovery, although the positive trend based on PWLT is not statistically significant. Compared to the zonal mean trend over the same latitude band, the TP ozone trend shows a relatively smaller rate of increase after 1997, which highlights the zonal asymmetry in ozone recovery.

- Overall, regression results based on three groups of independent explanatory variables show that the GH150 proxy improves the regression especially for the TP region, and is more significant than the ST proxy. By comparison of the contributions of different proxies in DJF and JJA, dynamical proxies (QBO and GH150) dominate the wintertime TCO variations over the TP, with statistical significance at 99% confidence level, but in summertime photochemical processes dominate and dynamical process decays (QBO at 10 hPa persists but GH150 disappears). The positive correlation between the DJF and JJA TCO over the TP indicates the seasonal persistence of total ozone variations from the ozone buildup in winter to the decreasing period in summer. Our analysis clearly highlights the influence of wintertime GH150 variations on summertime TCO trends.

- Results from the SLIMCAT control experiment R1 reproduce the TCO time series and regression results for the TP region, and are consistent with the C3S-based results. Sensitivity experiments R2 and R3 are performed to explore the significant contribution of the GH150 proxy to the wintertime Tibetan ozone variations. The composite analysis shows that GH150 fluctuations play a key role in controlling the DJF mean TCO variability over the TP, which may be associated with ITCZ, ENSO events or Walker circulation.

Overall, our results show that stratospheric ozone recovery due to the impact of the Montreal Protocol is not expected to behave similarly at all longitudes within a certain latitude region. In the specific case of the Tibetan Plateau, other local factors, which vary with season, will affect column ozone variations. Given, the impact of dynamical proxies described above, column ozone over the TP will be subject to long-term changes beyond halogenated ozone-depleting substances and needs careful monitoring.

Data availability. The satellite and climate data used in this study are available at the sources and references in the dataset section. The model data used are available upon request (w.feng@ncas.ac.uk).

Author contributions. YL performed the data analysis and prepared the manuscript. MPC, WF, SSD, RJP, GD and FL gave support for discussion, simulation and interpretation, and helped to write the paper. All authors edited and contributed to subsequent drafts of the manuscript.

Competing interests. The authors declare that they have no conflict of interest.

Acknowledgements. We are grateful to the Copernicus Climate Change Service (C3S) for providing the global ozone dataset. The modelling work is supported by National Centre for Atmospheric Science (NCAS). We thank all providers of the climate data used in this study. We thank Jiankai Zhang (Univ. Cambridge) and Dingzhu Hu (Univ. Reading) for helpful suggestions on the Tibetan ozone trends and regression analysis. We also acknowledge the support of National Natural Science Foundation of China (Grant No. 41127901), Jiangsu provincial government scholarship programme and the Natural Science Foundation for universities in Jiangsu province (Grant No. 17KJD170004).

References

Austin, J., Scinocca, J., Plummer, D., Oman, L., Waugh, D., Akiyoshi, H., Bekki, S., Braesicke, P., Butchart, N., Chipperfield, M., Cugnet, D., Dameris, M., Dhomse, S., Eyring, V., Frith, S., Garcia, R. R., Garny, H., Gettelman, A., Hardiman, S. C., Kinnison, D., Lamarque, J. F., Mancini, E., Marchand, M., Michou, M., Morgenstern, O., Nakamura, T., Pawson, S., Pitari, G., Pyle, J., Rozanov, E., Shepherd, T. G., Shibata, K., Teyssedre, H., Wilson, R. J., and Yamashita, Y.: Decline and recovery of total column ozone using a multimodel time series analysis, Journal of Geophysical Research-Atmospheres, 115, 10.1029/2010jd013857, 2010.

Baldwin, M. P., Gray, L. J., Dunkerton, T. J., Hamilton, K., Haynes, P. H., Randel, W. J., Holton, J. R., Alexander, M. J., Hirota, I., Horinouchi, T., Jones, D. B. A., Kinnersley, J. S., Marquardt, C., Sato, K., and Takahashi, M.: The quasi-biennial oscillation, Reviews of Geophysics, 39, 179-229, 10.1029/1999rg000073, 2001.

Bian, J. C., Wang, G. C., Chen, H. B., Qi, D. L., Lu, D., and Zhou, X. J.: Ozone mini-hole occurring over the Tibetan Plateau in December 2003, Chinese Science Bulletin, 51, 885-888, 10.1007/s11434-006-0885-y, 2006.

Bian, J. C., Yan, R. C., Chen, H. B., Lu, D. R., and Massie, S. T.: Formation of the Summertime Ozone Valley over the Tibetan Plateau: The Asian Summer Monsoon and Air Column Variations, Advances in Atmospheric Sciences, 28, 1318-1325, 10.1007/s00376-011-0174-9, 2011.

Camp, C. D., and Tung, K. K.: Stratospheric polar warming by ENSO in winter: A statistical study, Geophysical Research Letters, 34, 10.1029/2006gl028521, 2007.

Chehade, W., Weber, M., and Burrows, J. P.: Total ozone trends and variability during 1979-2012 from merged data sets of various satellites, Atmospheric Chemistry and Physics, 14, 7059-7074, 10.5194/acp-14-7059-2014, 2014.

Chipperfield, M. P.: New version of the TOMCAT/SLIMCAT off-line chemical transport model: Intercomparison of stratospheric tracer experiments, Quarterly Journal of the Royal Meteorological Society, 132, 1179-1203, 10.1256/qj.05.51, 2006.

Chipperfield, M. P., Dhomse, S. S., Feng, W., McKenzie, R. L., Velders, G. J. M., and Pyle, J.

A.: Quantifying the ozone and ultraviolet benefits already achieved by the Montreal Protocol, Nature Communications, 6, 10.1038/ncomms8233, 2015.

Chipperfield, M. P., Bekki, S., Dhomse, S., Harris, N. R. P., Hassler, B., Hossaini, R., Steinbrecht, W., Thieblemont, R., and Weber, M.: Detecting recovery of the stratospheric ozone layer, Nature, 549, 211-218, 10.1038/nature23681, 2017.

Chipperfield, M. P., Dhomse, S., Hossaini, R., Feng, W. H., Santee, M. L., Weber, M., Burrows, J. P., Wild, J. D., Loyola, D., and Coldewey-Egbers, M.: On the Cause of Recent Variations in Lower Stratospheric Ozone, Geophysical Research Letters, 45, 5718-5726, 10.1029/2018gl078071, 2018.

Christidis, N., and Stott, P. A.: Changes in the geopotential height at 500 hPa under the influence of external climatic forcings, Geophysical Research Letters, 42, 10,798-710,806, 10.1002/2015gl066669, 2015.

Dee, D. P., Uppala, S. M., Simmons, A. J., Berrisford, P., Poli, P., Kobayashi, S., Andrae, U., Balmaseda, M. A., Balsamo, G., Bauer, P., Bechtold, P., Beljaars, A. C. M., van de Berg, L., Bidlot, J., Bormann, N., Delsol, C., Dragani, R., Fuentes, M., Geer, A. J., Haimberger, L., Healy, S. B., Hersbach, H., Holm, E. V., Isaksen, L., Kallberg, P., Kohler, M., Matricardi, M., McNally, A. P., Monge-Sanz, B. M., Morcrette, J. J., Park, B. K., Peubey, C., de Rosnay, P., Tavolato, C., Thepaut, J. N., and Vitart, F.: The ERA-Interim reanalysis: configuration and performance of the data assimilation system, Quarterly Journal of the Royal Meteorological Society, 137, 553-597, 10.1002/qj.828, 2011.

Dhomse, S., Weber, M., Wohltmann, I., Rex, M., and Burrows, J. P.: On the possible causes of recent increases in northern hemispheric total ozone from a statistical analysis of satellite data from 1979 to 2003, Atmospheric Chemistry and Physics, 6, 1165-1180, 10.5194/acp-6-1165-2006, 2006.

Dhomse, S., Chipperfield, M. P., Feng, W., and Haigh, J. D.: Solar response in tropical stratospheric ozone: a 3-D chemical transport model study using ERA reanalyses, Atmospheric Chemistry and Physics, 11, 12773-12786, 10.5194/acp-11-12773-2011, 2011.

Dhomse, S. S., Chipperfield, M. P., Feng, W., Ball, W. T., Unruh, Y. C., Haigh, J. D., Krivova, N. A., Solanki, S. K., and Smith, A. K.: Stratospheric O-3 changes during 2001-2010: the small role of solar flux variations in a chemical transport model, Atmospheric Chemistry and Physics, 13, 10113-10123, 10.5194/acp-13-10113-2013, 2013.

Dhomse, S. S., Chipperfield, M. P., Feng, W., Hossaini, R., Mann, G. W., and Santee, M. L.: Revisiting the hemispheric asymmetry in mid-latitude ozone changes following the Mount Pinatubo eruption: A 3-D model study, Geophysical Research Letters, 42, 3038-3047, 10.1002/2015gl063052, 2015.

Dhomse, S. S., Chipperfield, M. P., Damadeo, R. P., Zawodny, J. M., Ball, W. T., Feng, W., Hossaini, R., Mann, G. W., and Haigh, J. D.: On the ambiguous nature of the 11year solar cycle signal in upper stratospheric ozone, Geophysical Research Letters, 43, 7241-7249, 10.1002/2016gl069958, 2016.

Farman, J. C., Gardiner, B. G., and Shanklin, J. D.: Large losses of total ozone in Antarctica reveal sea- sonal ClOx/NOx interaction, Nature, 315, 207-210, 10.1038/315207a0, 1985.

Feng, W., Chipperfield, M. P., Davies, S., Mann, G. W., Carslaw, K. S., Dhomse, S., Harvey, L., Randall, C., and Santee, M. L.: Modelling the effect of denitrification on polar ozone depletion for Arctic winter 2004/2005, Atmospheric Chemistry and Physics, 11, 6559-6573, 10.5194/acp-11-6559-2011, 2011.

Fioletov, V. E., and Shepherd, T. G.: Seasonal persistence of mid-latitude total ozone anomalies, Geophysical Research Letters, 30, doi:10.1029/2002gl016739, 2003.

Fioletov, V. E., and Shepherd, T. G.: Summertime total ozone variations over middle and polar latitudes, Geophysical Research Letters, 32, 10.1029/2004gl022080, 2005.

Fioletov, V. E.: Estimating the 27-day and 11-year solar cycle variations in tropical upper stratospheric ozone, Journal of Geophysical Research-Atmospheres, 114, 10.1029/2008jd010499, 2009.

Forster, P. M. D., and Shine, K. P.: Radiative forcing and temperature trends from stratospheric ozone changes, Journal of Geophysical Research-Atmospheres, 102, 10841-10855, 10.1029/96jd03510, 1997.

Frith, S. M., Kramarova, N. A., Stolarski, R. S., McPeters, R. D., Bhartia, P. K., and Labow, G. J.: Recent changes in total column ozone based on the SBUV Version 8.6 Merged Ozone Data Set, Journal of Geophysical Research-Atmospheres, 119, 9735-9751, 10.1002/2014jd021889, 2014.

Fusco, A. C., and Salby, M. L.: Interannual variations of total ozone and their relationship to variations of planetary wave activity, Journal of Climate, 12, 1619-1629, 10.1175/1520-0442(1999)012<1619:ivotoa>2.0.co;2, 1999.

Gettelman, A., Kinnison, D. E., Dunkerton, T. J., and Brasseur, G. P.: Impact of monsoon circulations on the upper troposphere and lower stratosphere, Journal of Geophysical Research-Atmospheres, 109, 14, doi:10.1029/2004jd004878, 2004.

Grooss, J. U., Muller, R., Spang, R., Tritscher, I., Wegner, T., Chipperfield, M. P., Feng, W. H., Kinnison, D. E., and Madronich, S.: On the discrepancy of HCl processing in the core of the wintertime polar vortices, Atmospheric Chemistry and Physics, 18, 8647-8666, 10.5194/acp-18-8647-2018, 2018.

Guo, D., Wang, P. X., Zhou, X. J., Liu, Y., and Li, W. L.: Dynamic Effects of the South Asian High on the Ozone Valley over the Tibetan Plateau, Acta Meteorologica Sinica, 26, 216-228, 10.1007/s13351-012-0207-2, 2012.

Guo, D., Su, Y. C., Shi, C. H., Xu, J. J., and Powell, A. M.: Double core of ozone valley over the Tibetan Plateau and its possible mechanisms, Journal of Atmospheric and Solar-Terrestrial Physics, 130, 127-131, 10.1016/j.jastp.2015.05.018, 2015.

Harris, N. R. P., Kyro, E., Staehelin, J., Brunner, D., Andersen, S. B., Godin-Beekmann, S., Dhomse, S., Hadjinicolaou, P., Hansen, G., Isaksen, I., Jrrar, A., Karpetchko, A., Kivi, R., Knudsen, B., Krizan, P., Lastovicka, J., Maeder, J., Orsolini, Y., Pyle, J. A., Rex, M., Vanicek, K., Weber, M., Wohltmann, I., Zanis, P., and Zerefos, C.: Ozone trends at northern mid- and high latitudes - a European perspective, Annales Geophysicae, 26, 1207-1220, 10.5194/angeo-26-1207-2008, 2008.

Hartmann, D. L., Wallace, J. M., Limpasuvan, V., Thompson, D. W. J., and Holton, J. R.: Can ozone depletion and global warming interact to produce rapid climate change?, Proceedings of the National Academy of Sciences of the United States of America, 97, 1412-1417, 10.1073/pnas.97.4.1412, 2000.

Holton, J. R., and Tan, H. C.: The Influence of the Equatorial Quasi-Biennial Oscillation on the Global Circulation at 50 mb, Journal of the Atmospheric Sciences, 37, 2200-2208, doi:10.1175/1520-0469(1980)037<2200:Tioteq>2.0.Co;2, 1980.

Hood, L. L., and Soukharev, B. E.: Interannual variations of total ozone at northern mid-latitudes correlated with stratospheric EP flux and potential vorticity, Journal of the Atmospheric

Sciences, 62, 3724-3740, 10.1175/jas3559.1, 2005.

Hu, D. Z., Tian, W. S., Guan, Z. Y., Guo, Y. P., and Dhomse, S.: Longitudinal Asymmetric Trends of Tropical Cold-Point Tropopause Temperature and Their Link to Strengthened Walker Circulation, Journal of Climate, 29, 7755-7771, 10.1175/jcli-d-15-0851.1, 2016.

Labow, G. J., McPeters, R. D., Bhartia, P. K., and Kramarova, N.: A comparison of 40 years of SBUV measurements of column ozone with data from the Dobson/Brewer network, Journal of Geophysical Research-Atmospheres, 118, 7370-7378, doi:10.1002/jgrd.50503, 2013.

Liu, Y., Li, W. L., Zhou, X. J., and He, J. H.: Mechanism of formation of the ozone valley over the Tibetan plateau in summer-transport and chemical process of ozone, Advances in Atmospheric Sciences, 20, 103-109, 10.1007/bf03342054, 2003.

Luo, J. L., Liang, W. J., Xu, P. P., Xue, H. Y., Zhang, M., Shang, L., and Tian, H. Y.: Seasonal Features and a Case Study of Tropopause Folds over the Tibetan Plateau, Advances in Meteorology, 2019, doi:10.1155/2019/4375123, 2019.

McLandress, C., Plummer, D. A., and Shepherd, T. G.: Technical Note: A simple procedure for removing temporal discontinuities in ERA-Interim upper stratospheric temperatures for use in nudged chemistry-climate model simulations, Atmospheric Chemistry and Physics, 14, 1547-1555, 10.5194/acp-14-1547-2014, 2014.

Nair, P. J., Godin-Beekmann, S., Kuttippurath, J., Ancellet, G., Goutail, F., Pazmiño, A., Froidevaux, L., Zawodny, J. M., Evans, R. D., Wang, H. J., Anderson, J., and Pastel, M.: Ozone trends derived from the total column and vertical profiles at a north- ern mid-latitude station, Atmos. Chem. Phys., 13, 10373–10384, 10.5194/acp-13-10373-2013, 2013.

Newman, P. A., Kawa, S. R., and Nash, E. R.: On the size of the Antarctic ozone hole, Geophys. Res. Lett., 31, L21104, 10.1029/2004GL020596, 2004.

Randel, W. J., and Park, M.: Deep convective influence on the Asian summer monsoon anticyclone and associated tracer variability observed with Atmospheric Infrared Sounder (AIRS), Journal of Geophysical Research-Atmospheres, 111, 13, doi:10.1029/2005jd006490, 2006.

Randel, W. J., and Wu, F.: A stratospheric ozone profile data set for 1979-2005: Variability, trends, and comparisons with column ozone data, Journal of Geophysical Research-Atmospheres, 112, 10.1029/2006jd007339, 2007.

Reinsel, G. C., Weatherhead, E. C., Tiao, G. C., Miller, A. J., Nagatani, R. M., Wuebbles, D. J., and Flynn, L. E.: On detection of turnaround and recovery in trend for ozone, Journal of Geophysical Research-Atmospheres, 107, 10.1029/2001jd000500, 2002.

Rex, M., Salawitch, R. J., von der Gathen, P., Harris, N. R. P., Chipperfield, M. P., and Naujokat, B.: Arctic ozone loss and climate change, Geophysical Research Letters, 31, 10.1029/2003gl018844, 2004.

Shepherd, T. G., Plummer, D. A., Scinocca, J. F., Hegglin, M. I., Fioletov, V. E., Reader, M. C., Remsberg, E., von Clarmann, T., and Wang, H. J.: Reconciliation of halogen-induced ozone loss with the total-column ozone record, Nature Geoscience, 7, 443-449, 10.1038/ngeo2155, 2014.

Sofieva, V. F., Kyrola, E., Laine, M., Tamminen, J., Degenstein, D., Bourassa, A., Roth, C., Zawada, D., Weber, M., Rozanov, A., Rahpoe, N., Stiller, G., Laeng, A., von Clarmann, T., Walker, K. A., Sheese, P., Hubert, D., van Roozendael, M., Zehner, C., Damadeo, R., Zawodny, J., Kramarova, N., and Bhartia, P. K.: Merged SAGE II, Ozone_cci and OMPS ozone profile dataset and evaluation of ozone trends in the stratosphere, Atmospheric

Chemistry and Physics, 17, 12533-12552, 10.5194/acp-17-12533-2017, 2017.
Solomon, S., Ivy, D. J., Kinnison, D., Mills, M. J., Neely, R. R., and Schmidt, A.: Emergence of healing in the Antarctic ozone layer, Science, 353, 269-274, 10.1126/science.aae0061, 2016.
Soukharev, B. E., and Hood, L. L.: Solar cycle variation of stratospheric ozone: Multiple regression analysis of long-term satellite data sets and comparisons with models, Journal of Geophysical Research-Atmospheres, 111, 10.1029/2006jd007107, 2006.
Steinbrecht, W., Froidevaux, L., Fuller, R., Wang, R., Anderson, J., Roth, C., Bourassa, A., Degenstein, D., Damadeo, R., Zawodny, J., Frith, S., McPeters, R., Bhartia, P., Wild, J., Long, C., Davis, S., Rosenlof, K., Sofieva, V., Walker, K., Rahpoe, N., Rozanov, A., Weber, M., Laeng, A., von Clarmann, T., Stiller, G., Kramarova, N., Godin-Beekmann, S., Leblanc, T., Querel, R., Swart, D., Boyd, I., Hocke, K., Kampfer, N., Barras, E. M., Moreira, L., Nedoluha, G., Vigouroux, C., Blumenstock, T., Schneider, M., Garcia, O., Jones, N., Mahieu, E., Smale, D., Kotkamp, M., Robinson, J., Petropavlovskikh, I., Harris, N., Hassler, B., Hubert, D., and Tummon, F.: An update on ozone profile trends for the period 2000 to 2016, Atmospheric Chemistry and Physics, 17, 10675-10690, 10.5194/acp-17-10675-2017, 2017.
Tian, W., Chipperfield, M., and Huang, Q.: Effects of the Tibetan Plateau on total column ozone distribution, Tellus Series B-Chemical and Physical Meteorology, 60, 622-635, 10.1111/j.1600-0889.2008.00338.x, 2008.
Tobo, Y., Iwasaka, Y., Zhang, D., Shi, G., Kim, Y. S., Tamura, K., and Ohashi, T.: Summertime "ozone valley" over the Tibetan Plateau derived from ozonesondes and EP/TOMS data, Geophysical Research Letters, 35, 10.1029/2008gl034341, 2008.
Weber, M., Dhomse, S., Wittrock, F., Richter, A., Sinnhuber, B. M., and Burrows, J. P.: Dynamical control of NH and SH winter/spring total ozone from GOME observations in 1995-2002, Geophysical Research Letters, 30, 10.1029/2002gl016799, 2003.
Weber, M., Coldewey-Egbers, M., Fioletov, V. E., Frith, S. M., Wild, J. D., Burrows, J. P., Long, C. S., and Loyola, D.: Total ozone trends from 1979 to 2016 derived from five merged observational datasets - the emergence into ozone recovery, Atmospheric Chemistry and Physics, 18, 2097-2117, 10.5194/acp-18-2097-2018, 2018.
WMO: Scientific Assessment of Ozone Depletion: 2014. Global Ozone Research and Monitoring Project-Report No. 55, Geneva, Switzerland, 2014.
Yanai, M. H., Li, C. F., and Song, Z. S.: Seasonal heating of the Tibetan Plateau and its effects on the evolution of the Asian summer monsoon, Journal of the Meteorological Society of Japan, 70, 319-351, 10.2151/jmsj1965.70.1B_319, 1992.
Ye, D. Z., and Wu, G. X.: The role of the heat source of the Tibetan Plateau in the general circulation, Meteorology and Atmospheric Physics, 67, 181-198, 10.1007/bf01277509, 1998.
Ye, Z. J., and Xu, Y. F.: Climate characteristics of ozone over Tibetan Plateau, Journal of Geophysical Research-Atmospheres, 108, 10.1029/2002jd003139, 2003.
Zhang, J. K., Tian, W. S., Xie, F., Tian, H. Y., Luo, J. L., Zhang, J., Liu, W., and Dhomse, S.: Climate warming and decreasing total column ozone over the Tibetan Plateau during winter and spring, Tellus Series B-Chemical and Physical Meteorology, 66, 10.3402/tellusb.v66.23415, 2014.
Zhang, J. K., Tian, W. S., Xie, F., Chipperfield, M. P., Feng, W. H., Son, S. W., Abraham, N. L., Archibald, A. T., Bekki, S., Butchart, N., Deushi, M., Dhomse, S., Han, Y. Y., Jockel, P., Kinnison, D., Kirner, O., Michou, M., Morgenstern, O., O'Connor, F. M., Pitari, G., Plummer, D. A., Revell, L. E., Rozanov, E., Visioni, D., Wang, W. K., and Zeng, G.: Stratospheric ozone

loss over the Eurasian continent induced by the polar vortex shift, Nature Communications, 9, 10.1038/s41467-017-02565-2, 2018.

Zhang, J. K., Tian, W. S., Xie, F., Sang, W. J., Guo, D., Chipperfield, M., Feng, W. H., and Hu, D. Z.: Zonally asymmetric trends of winter total column ozone in the northern middle latitudes, Climate Dynamics, 52, 4483-4500, 10.1007/s00382-018-4393-y, 2019.

Zheng, X. D., Zhou, X. J., Tang, J., Qin, Y., and Chan, C. Y.: A meteorological analysis on a low tropospheric ozone event over Xining, North Western China on 26-27 July 1996, Atmospheric Environment, 38, 261-271, 10.1016/j.atmosenv.2003.09.063, 2004.

Zhou, L. B., Zou, H., Ma, S. P., and Li, P.: The Tibetan ozone low and its long-term variation during 1979-2010, Acta Meteorologica Sinica, 27, 75-86, 10.1007/s13351-013-0108-9, 2013.

Zhou, S. W., and Zhang, R. H.: Decadal variations of temperature and geopotential height over the Tibetan Plateau and their relations with Tibet ozone depletion, Geophysical Research Letters, 32, 10.1029/2005gl023496, 2005.

Zhou, X., Lou, C., Li, W. L. and Shi, J. E: Ozone changes over China and low center over Tibetan Plateau, Chin. Sci. Bull., 40, 1396-1398, 1995.

Ziemke, J. R., Chandra, S., McPeters, R. D., and Newman, P. A.: Dynamical proxies of column ozone with applications to global trend models, Journal of Geophysical Research-Atmospheres, 102, 6117-6129, 10.1029/96jd03783, 1997.

Zou, H.: Seasonal variation and trends of TOMS ozone over Tibet, Geophysical Research Letters, 23, 1029-1032, 10.1029/96gl00767, 1996.

Zou, H., Ji, C. P., and Zhou, L. B.: QBO signal in total ozone over Tibet, Advances in Atmospheric Sciences, 17, 562-568, 2000.

Zou, H., Ji, C. P., Zhou, L. B., Wang, W., and Jian, Y. X.: ENSO signal in total ozone over Tibet, Advances in Atmospheric Sciences, 18, 231-238, 2001.

Zvyagintsev, A. M., Vargin, P. N., and Peshin, S.: Total Ozone Variations and Trends during the Period 1979-2014, Atmospheric and Oceanic Optics, 28, 575-584, 10.1134/s1024856015060196, 2015.